Journal of Power Sources 186 (2009) 435–445

Contents lists available at ScienceDirect

Journal of Power Sources

journal homepage: www.elsevier.com/locate/jpowsour

A general model for air-side proton exchange membrane fuel cell contamination

Zheng Shi*, Datong Song, Hui Li, Khalid Fatih, Yanghua Tang, Jianlu Zhang, Zhenwei Wang, Shaohong Wu, Zhong-Sheng Liu, Haijiang Wang, Jiujun Zhang

Institute for Fuel Cell Innovation, National Research Council of Canada, Vancouver, BC, Canada V6T 1W5

ARTICLE INFO

Article history:
Received 19 August 2008
Received in revised form
30 September 2008
Accepted 1 October 2008
Available online 17 October 2008

Keywords:
PEM fuel cells
Air contaminants and impurities
Contamination model
Toluene
Oxygen reduction reaction mechanism
Degradation

ABSTRACT

This paper presents a general model for air-side feed stream contamination that has the capability of simulating both transient and steady-state performance of a PEM fuel cell in the presence of air-side feed stream impurities. The model is developed based on the oxygen reduction reaction mechanism, contaminant surface adsorption/desorption, and electrochemical reaction kinetics. The model is then applied to the study of air-side toluene contamination. Experimental data for toluene contamination at four current densities (0.2, 0.5, 0.75 and 1.0 A cm^{-2}) and three contamination levels (1, 5 and 10 ppm) were used to validate the model. In addition, it is expected that, with parameter adjustment, this model can also be used to predict performance degradation caused by other air impurities such as nitrogen oxides (NO_x) and sulfur oxides (SO_x).

1. Introduction

Proton exchange membrane fuel cell (PEMFC) contamination caused by impurities is an important issue in fuel cell operation and applications. Contaminants can be classified into two categories according to the source: external and hardware. External impurities enter the fuel cell mainly through the fuel or air feed stream. The major impurities in hydrogen fuel produced from reformate include CO, CO_2, H_2S, NH_3, organic sulfur–carbon, and carbon–hydrogen compounds, and those in air include pollutants such as NO_x, SO_x, NH_3, O_3 and small organic compounds. The impurities introduced through hardware sources contain metal ions such as Fe^{3+}, Cu^{2+}, Ni^{2+}, and Cr^{3+} from gas diffusion layers, bipolar plates, and system components, Na, Ca, and S from membranes, and Si from gaskets and cooling fluid.

It has been demonstrated that even trace amounts of impurities in the fuel or air stream or the fuel cell system components can severely poison the anode, membrane, and cathode, particularly at low-temperature operation. The contaminants can: strongly or irreversibly adsorb on the catalyst surface, blocking the reaction sites; enter the membrane, reducing proton conductivity; and change the hydrophobicity/hydrophilicity of the catalyst layer interface, affecting mass transportation. As a result, contaminants cause performance degradation and sometimes permanent damage to the membrane electrode assemblies (MEAs) [1–3]. To address this issue, a great deal of effort has been put into identifying the potential impacts of contamination, understanding the contamination mechanisms, and developing mitigation strategies.

At present, contamination research concentrates on three major areas: (1) experimental impact observation and validation; (2) theoretical modeling of contamination to provide a fundamental understanding of the mechanisms and to develop predictive tools; and (3) contamination mitigation strategy development. With respect to contamination impact observation, the effects on fuel cell performance of impurities such as CO, CO_2, H_2S, and NH_3 in the fuel feed [4–20] and SO_x, NO_x, H_2S, and NH_3 [16,21–24] in the air stream have been extensively examined. A study of battlefield air impurities such as benzene, propane, HCN, CNCL, sarin, and sulfur mustard has also been reported [25]. In terms of model development for predicting fuel cell contamination, numerous studies on fuel cell contamination have been conducted, especially for CO contamination [26–37]. For fuel-side H_2S contamination, a kinetic model has been developed to study both transient and steady fuel cell performance [38]. But to the best of our knowledge a comprehensive predictive model for air-side feed stream contamination is not yet available in the literature, other than a preliminary adsorption model for NO_2 [39]. Since air pollutants have a large effect on fuel cell applications, for example, portable power units for indoor

* Corresponding author. Tel.: +1 604 221 3000.
E-mail address: zheng.shi@nrc.gc.ca (Z. Shi).

0378-7753/$ – see front matter.
doi:10.1016/j.jpowsour.2008.10.029

Nomenclature

C_{O_2}	oxygen concentration in the catalyst layer
C_{H^+}	proton concentration in the CCL
C_P	concentration of species P
$C_{P'}$	concentration of species P′
C_P^0	contaminant concentration in the cathode channel
$D_{O_2,air}$	bulk oxygen diffusivity
$D_{O_2,air}^{eff}$	effective oxygen diffusivity
F	Faraday's constant
I_{cell}	cell current density
k_{a3f} and k_{a3b}	forward and backward reaction rates of the reaction (a-iii)
k_{ap3f} and k_{ap3b}	forward and backward reaction rates of the reaction (a-vi)
k_{jf} and k_{jb}	forward and backward reaction rates of the jth reaction (j = 1, 2, . . ., 5)
k_{pjf} and k_{pjb}	forward and backward reaction rates of the reactions (a-iv), (a-v), (a-vii) and (a-viii) (j = 1, 2, 4, 5)
L_{CGDL}	thickness of the cathode gas diffusion layer
n	number of the Pt sites occupied by contaminant P
n_j	electron transfer number for the corresponding individual electrochemical half-reaction (j = 1, 2, . . ., 5)
n_{a3}	electron transfer number
n_{ap3}	electron transfer number of the reaction (a-vi)
n_{O_2}	electron transfer number of the ORR
p_{O_2}	oxygen partial pressure
p_{CGC}	gas pressure in gas channel
p_{vapor}^{sat}	saturated water vapor pressure
q	electron transfer number of the reaction (a-vii)
R	ideal gas constant
R_0	fuel cell internal resistance (membrane resistance)
t	time
T	temperature
V_{cell}	cell voltage
V^0	open circuit voltage (OCV)
z	electron transfer number of the reaction (a-viii)

Greek symbols

α_j	electron transfer coefficient for the corresponding individual electrochemical half-reaction, j = 1, 2, . . ., 5
α_{a3}	electron transfer coefficient of the electrochemical half-reaction
α_{ap3}, α_{p4} and α_{p5}	electron transfer coefficients of reactions (a-vi), (a-vii) and (a-viii)
Γ	total surface
γ_c	ratio of the active surface to the geometric surface of the CCL
ε_{CGDL}	porosity of the cathode gas diffusion layer
η_a	anode overpotential
η_c	cathode overpotential
θ_{Pt}, θ_{Pt-O_2}, θ_{Pt-O_2H}, θ_{Pt_n-P} and $\theta_{Pt_n-P'}$	surface coverages of corresponding species
θ_{Pt}^0, $\theta_{Pt-O_2}^0$ and $\theta_{Pt-O_2H}^0$	surface coverages of corresponding species without contaminant

and underground applications and fleet vehicles for outdoor applications, developing a predictive model for air-side contamination is necessary in order to evaluate fuel cell performance under the above-mentioned conditions.

In this paper, we present our work on the development of a general model for fuel cell air-side feed stream contamination. This is a kinetic model that is mainly based on the proposed oxygen reduction mechanisms, the contaminant's surface adsorption, and the electrode reaction mechanism. The model has the capability to simulate both transient and steady-state cell performance in the presence of an air contaminant. The model is further validated by our experimental data collected in the presence of toluene in a fuel cell air-side feed stream. These experimental data were obtained at different current densities and several toluene contamination levels. The model is further employed to examine the toluene contamination effect on cell performance at low concentration levels.

2. Model development

2.1. Oxygen reduction reaction

The oxygen reduction reaction (ORR) is a multi-electron multi-step reaction. For the ORR on a platinum (Pt) surface, two Tafel regions are generally observed in both acidic and alkaline solutions. At low current densities (high electrode potential), a Tafel slope of −60 mV dec^{-1} can be observed, whereas high current densities (low electrode potential) yield a Tafel slope of −120 mV dec^{-1} [40]. The difference in Tafel slopes is attributable to partial coverage of the Pt surface by the oxygen-containing intermediates O and OH. Experimental study indicates that the reaction rate is first order with respect to oxygen. Extensive research of the ORR on Pt surfaces has been conducted in the past 40 or so years and a considerable number of ORR mechanisms have been proposed [41–44]. Yet despite numerous studies of the ORR, the detailed mechanism remains elusive. Damjanovic and co-workers [40,45,46] proposed that the charge transfer to the adsorbed oxygen molecule, with or without simultaneous proton transfer, is the rate-determining step (associative model):

$$M + O_2 \rightarrow M\text{–}O_2 \quad (1)$$

$$M\text{–}O_2 + H^+ + e^- \rightarrow M\text{–}O_2H(rds) \quad (2)$$

$$M\text{–}O_2H + 3H^+ + 3e^- \rightarrow 2H_2O + M \quad (3)$$

where M represents a metal such as Pt. Yeager et al. [47] proposed that the first step involves dissociative chemisorption of the O_2 molecule, which occurs simultaneously with the charge transfer (dissociative model):

$$Pt + \tfrac{1}{2}O_2 + e^- \rightarrow Pt\text{–}O^- \quad (4)$$

In the search to understand ORR mechanisms, several model-based impedance spectroscopy studies were reported that employed either an associative kinetic model or a dissociative one [48–50]. In another kinetic model study [51], both associative and dissociative mechanisms were analyzed.

In recent years, many theoretical explorations of the ORR mechanism using quantum mechanic methods have been reported, as shown in the review articles [52,53]. These studies supplied information on each elementary step, such as activation energies, reaction energies, and reversible potentials. Anderson and co-workers [54,55] investigated the activation barrier for each of the following electron transfer steps:

$$Pt\text{–}O_2 + H^+(aq) + e^- \quad (U) \rightarrow Pt\text{–}OOH \quad (5)$$

$$Pt\text{–}OOH + H^+(aq) + e^- \quad (U) \rightarrow Pt\text{–}(OHOH) \quad (6)$$

$$\mathrm{Pt{-}OHOH} + \mathrm{H^+(aq)} + \mathrm{e^-} \quad (\mathrm{U}) \rightarrow \mathrm{Pt{-}OH} + \mathrm{H_2O} \tag{7}$$

$$\mathrm{Pt{-}OH} + \mathrm{H^+(aq)} + \mathrm{e^-} \quad (\mathrm{U}) \rightarrow \mathrm{Pt{-}OH_2} \tag{8}$$

Their results showed that the first electron transfer has a smaller activation energy barrier than that of oxygen dissociation, and that OOH easily dissociates once formed after the first electron transfer.

Norskov et al. [56,57] examined the thermodynamic properties of both associative and dissociative mechanisms:

$$\tfrac{1}{2}\mathrm{O_2} + {}^* \rightarrow \mathrm{O^*} \tag{9}$$

$$\mathrm{O^*} + \mathrm{H^+} + \mathrm{e^-} \rightarrow \mathrm{HO^*} \tag{10}$$

$$\mathrm{HO^*} + \mathrm{H^+} + \mathrm{e^-} \rightarrow \mathrm{H_2O} + {}^* \tag{11}$$

where * denotes a site on the surface.

$$\mathrm{O_2} + {}^* \rightarrow \mathrm{O_2{}^*} \tag{12}$$

$$\mathrm{O_2{}^*} + (\mathrm{H^+} + \mathrm{e^-}) \rightarrow \mathrm{HO_2{}^*} \tag{13}$$

$$\mathrm{HO_2{}^*} + (\mathrm{H^+} + \mathrm{e^-}) \rightarrow \mathrm{H_2O} + \mathrm{O^*} \tag{14}$$

$$\mathrm{O^*} + (\mathrm{H^+} + \mathrm{e^-}) \rightarrow \mathrm{HO^*} \tag{15}$$

$$\mathrm{HO^*} + (\mathrm{H^+} + \mathrm{e^-}) \rightarrow \mathrm{H_2O} + {}^* \tag{16}$$

The results illustrated that both mechanisms are possible and are controlled by electrode potential. At high electrode potential, the activation energy barrier for O_2 dissociation will increase; thus, the associative mechanism is dominant. Jacob's study [58] also demonstrated that both the associative and the dissociative mechanism may occur simultaneously, with a higher ratio of occurrence for the associative pathway. In another theoretical study [59], Walch et al. formulated a suitable mechanism table for the prominent ORR pathway. This mechanism includes chemical, electrochemical, and side reactions as follows:

Chemical reaction:

$$\mathrm{O_{2(ads)}} \leftrightarrow \mathrm{O_{(ads)}} + \mathrm{O_{(ads)}} \tag{17}$$

$$\mathrm{O_2H_{(ads)}} \leftrightarrow \mathrm{O_{(ads)}} + \mathrm{OH_{(ads)}} \tag{18}$$

$$\mathrm{H_2O_{(ads)}} \leftrightarrow \mathrm{H_{(ads)}} + \mathrm{HO_{(ads)}} \tag{19}$$

$$\mathrm{OH_{(ads)}} + \mathrm{OH_{(ads)}} \leftrightarrow \mathrm{O_{(ads)}} + \mathrm{H_2O_{(ads)}} \tag{20}$$

$$\mathrm{OH_{(ads)}} + \mathrm{O_{(ads)}} \leftrightarrow \mathrm{O_{(ads)}} + \mathrm{OH_{(ads)}} \tag{21}$$

Electrochemical reaction:

$$\mathrm{O_{2(ads)}} + \mathrm{H^+_{(aq)}} + \mathrm{e^-} \leftrightarrow \mathrm{O_2H_{(ads)}} \tag{22}$$

$$\mathrm{OH_{(ads)}} + \mathrm{H^+_{(aq)}} + \mathrm{e^-} \leftrightarrow \mathrm{H_2O_{(ads)}} \tag{23}$$

$$\mathrm{O_{(ads)}} + \mathrm{H^+_{(aq)}} + \mathrm{e^-} \leftrightarrow \mathrm{OH_{(ads)}} \tag{24}$$

$$\mathrm{H_2O_{(ads)}} \leftrightarrow \mathrm{O_{(ads)}} + 2\mathrm{H^+_{(aq)}} + 2\mathrm{e^-} \tag{25}$$

Side reaction:

$$\mathrm{Pt} \leftrightarrow \mathrm{Pt^{2+}_{(aq)}} + 2\mathrm{e^-} \tag{26}$$

$$\mathrm{Pt^{2+}_{(aq)}} + \mathrm{H_2O} \leftrightarrow \mathrm{PtO} + 2\mathrm{H^+_{(aq)}} \tag{27}$$

$$\mathrm{Pt^{2+}_{(aq)}} + \mathrm{H_2} \leftrightarrow \mathrm{Pt} + 2\mathrm{H^+_{(aq)}} \tag{28}$$

2.2. Proposed general cathode contamination model

In our attempt to develop a cathode contamination model, we start with a simple ORR mechanism. Since the associative model has substantial experimental and theoretical support, we adopt it and propose the following mechanism:

$$\mathrm{Pt} + \mathrm{O_2} \underset{k_{1b}}{\overset{k_{1f}}{\rightleftarrows}} \mathrm{Pt{-}O_2} \tag{i}$$

$$\mathrm{Pt{-}O_2} + \mathrm{H^+} + \mathrm{e^-} \underset{k_{2b}\exp(((1-\alpha_2)n_2F\eta_c/RT))}{\overset{k_{2f}\exp(-(\alpha_2 n_2 F\eta_c/RT))}{\rightleftarrows}} \mathrm{Pt{-}O_2H} \tag{ii}$$

$$\mathrm{Pt{-}O_2H} + \mathrm{e^-} + \mathrm{H^+} \underset{k_{3b}\exp(((1-\alpha_3)n_3F\eta_c)/RT)}{\overset{k_{3f}\exp(-(\alpha_3 n_3 F\eta_c/RT))}{\rightleftarrows}} \mathrm{H_2O} + \mathrm{Pt{-}O} \tag{iii}$$

$$\mathrm{Pt{-}O} + \mathrm{H^+} + \mathrm{e^-} \underset{k_{4b}\exp(((1-\alpha_4)n_4\eta_cF)/RT)}{\overset{k_{4f}\exp(-(\alpha_4 n_4\eta_c F/RT))}{\rightleftarrows}} \mathrm{Pt{-}OH} \tag{iv}$$

$$\mathrm{Pt{-}OH} + \mathrm{H^+} + \mathrm{e^-} \underset{k_{5b}\exp(((1-\alpha_5)n_5\eta_cF)/RT)}{\overset{k_{5f}\exp(-(\alpha_5 n_5\eta_c F/RT))}{\rightleftarrows}} \mathrm{Pt} + \mathrm{H_2O} \tag{v}$$

where Pt is the active site for oxygen adsorption, which may contain more than one Pt site, k_{jf} and k_{jb} are the forward and backward reaction rates of the jth reaction ($j = 1, 2, \ldots, 5$), α_j is the electron transfer coefficient for the corresponding individual electrochemical half-reaction, n_j is the electron transfer number for the corresponding individual electrochemical half-reaction, η_c is the cathode overpotential, and F, R and T are Faraday's constant, the universal gas constant, and cell temperature, respectively.

In our model, we further propose that the first electron transfer (reaction (ii)) is the rate-determining step. In this case, we can further simplify the model to

$$\mathrm{Pt} + \mathrm{O_2} \underset{k_{1b}}{\overset{k_{1f}}{\rightleftarrows}} \mathrm{Pt{-}O_2} \tag{a-i}$$

$$\mathrm{Pt{-}O_2} + \mathrm{H^+} + \mathrm{e^-} \underset{k_{2b}\exp(((1-\alpha_2)n_2F\eta_c)/RT)}{\overset{k_{2f}\exp(-(\alpha_2 n_2 F\eta_c/RT))}{\rightleftarrows}} \mathrm{Pt{-}O_2H} \tag{a-ii}$$

$$\mathrm{Pt{-}O_2H} + 3\mathrm{e^-} + 3\mathrm{H^+} \underset{k_{a3b}\exp(((1-\alpha_{a3})n_{a3}F\eta_c)/RT)}{\overset{k_{a3f}\exp(-(\alpha_{a3} n_{a3} F\eta_c/RT))}{\rightleftarrows}} 2\mathrm{H_2O} + \mathrm{Pt} \tag{a-iii}$$

where k_{a3f} and k_{a3b} are the forward and backward reaction rates of the reaction (a-iii), and α_{a3} and n_{a3} are the electron transfer coefficient and electron transfer number of the electrochemical half-reaction, respectively.

Reaction (a-ii) is the rate-determining step. The advantage of this simplified model is that we can use one intermediate coverage Pt–OOH as the total oxygen-containing intermediates coverage, which also includes Pt-O and Pt-OH.

For a general air-side contaminant P, we consider the following possible electrode and surface reactions:

$$n\mathrm{Pt} + \mathrm{P} \underset{k_{p1b}}{\overset{k_{p1f}}{\rightleftarrows}} \mathrm{Pt}_n\mathrm{{-}P} \tag{a-iv}$$

$$\mathrm{P} + n\mathrm{Pt{-}O_2} \underset{k_{p2b}}{\overset{k_{p2f}}{\rightleftarrows}} \mathrm{Pt}_n\mathrm{{-}P} + n\mathrm{O_2} \tag{a-v}$$

$$\mathrm{P} + n\mathrm{Pt{-}O_2H} + 3n\mathrm{e^-} + 3n\mathrm{H^+} \underset{k_{ap3b}\exp(((1-\alpha_{ap3})n_{ap3}F\eta_c)/RT)}{\overset{k_{ap3f}\exp(-(\alpha_{ap3} n_{ap3} F\eta_c/RT))}{\rightleftarrows}} 2n\mathrm{H_2O} + \mathrm{Pt}_n\mathrm{{-}P} \tag{a-vi}$$

$$\mathrm{Pt}_n\mathrm{{-}P} + m\mathrm{H_2O} \underset{k_{p4b}\exp(-((1-\alpha_{p4})qF\eta_c)/RT)}{\overset{k_{p4f}\exp((\alpha_{p4}qF\eta_c/RT))}{\rightleftarrows}} \mathrm{Pt}_n\mathrm{{-}P'} + \mathrm{qH^+} + \mathrm{qe^-} \tag{a-vii}$$

$$\mathrm{Pt}_n\mathrm{{-}P} + \mathrm{l\,H_2O} \underset{k_{p5b}\exp(-((1-\alpha_{p5})zF\eta_c)/RT)}{\overset{k_{p5f}\exp(\alpha_{p5}zF\eta_c/RT)}{\rightleftarrows}} n\mathrm{Pt} + \mathrm{P''} + \mathrm{zH^+} + \mathrm{ze^-} \tag{a-viii}$$

where Pt_n is the adsorption site for P.

Based on the proposed ORR and contaminant mechanisms, the Pt surface is covered by the following five species: Pt, Pt–O_2, Pt–O_2H, Pt$_n$–P and Pt$_n$–P′, where P′ is an oxidized form of P. Thus for the cathode catalyst surface coverage, we have

$$1 = \theta_{Pt} + \theta_{Pt\text{-}O_2} + \theta_{Pt\text{-}O_2H} + \theta_{Pt_n\text{-}P} + \theta_{Pt_n\text{-}P'} \quad (29)$$

where θ_{Pt}, $\theta_{Pt\text{-}O_2}$, $\theta_{Pt\text{-}O_2H}$, $\theta_{Pt_n\text{-}P}$ and $\theta_{Pt_n\text{-}P'}$ are the surface coverage of the above five species, respectively.

If we assume reaction (a-i) is fast and always at its equilibrium, we have

$$k_{1f} C_{O_2} \theta_{Pt} \Gamma = k_{1b} \theta_{Pt\text{-}O_2} \Gamma \quad (30)$$

where Γ is the total surface and C_{O_2} is the oxygen concentration in the cathode catalyst layer (CCL). We will have

$$\theta_{Pt\text{-}O_2} = \frac{k_{1f} C_{O_2}}{k_{1b}} \theta_{Pt} \quad (31)$$

Assuming reaction (a-iii) is always at its equilibrium,

$$k_{a3f} \theta_{Pt\text{-}O_2H} \Gamma C_{H^+}^3 \exp\left(-\frac{\alpha_{a3} n_{a3} \eta_c F}{RT}\right) = k_{a3b} \theta_{Pt} \Gamma \exp\left(\frac{(1-\alpha_{a3}) n_{a3} \eta_c F}{RT}\right) \quad (32)$$

where C_{H^+} is the proton concentration in the CCL. Solving the above equation for $\theta_{Pt\text{-}O_2H}$ results in

$$\theta_{Pt\text{-}O_2H} = \frac{k_{a3b}}{k_{a3f} C_{H^+}^3} \exp\left(\frac{n_{a3} \eta_c F}{RT}\right) \theta_{Pt} \quad (33)$$

Substituting Eqs. (31) and (33) into Eq. (29) and solving for θ_{Pt} yields

$$\theta_{Pt} = A(1 - \theta_{Pt_n\text{-}P} - \theta_{Pt_n\text{-}P'}) \quad (34)$$

where

$$A = \frac{1}{1 + \frac{k_{1f} C_{O_2}}{k_{1b}} + \frac{k_{a3b}}{k_{a3f} C_{H^+}^3} \exp\left(\frac{n_{a3} \eta_c F}{RT}\right)} \quad (35)$$

Let

$$B = \frac{k_{1f}}{k_{1b}} C_{O_2} A \quad (36)$$

and

$$C = \frac{k_{a3b}}{k_{a3f} C_{H^+}^3} \exp\left(\frac{n_{a3} \eta_c F}{RT}\right) A \quad (37)$$

Then the surface coverages of Pt–O_2 and Pt–O_2H are given as follows:

$$\theta_{Pt\text{-}O_2} = B(1 - \theta_{Pt_n\text{-}P} - \theta_{Pt_n\text{-}P'}) \quad (38)$$

and

$$\theta_{Pt\text{-}O_2H} = C(1 - \theta_{Pt_n\text{-}P} - \theta_{Pt_n\text{-}P'}) \quad (39)$$

If there is no contaminant present in the cathode catalyst layer (CCL), the surface coverages of Pt, Pt–O_2 and Pt–O_2H are only determined by the oxygen reduction reactions ((a-i), (a-ii) and (a-iii)) and are given as

$$\theta_{Pt}^0 = \frac{1}{1 + (k_{1f} C_{O_2}/k_{1b}) + (k_{a3b}/k_{a3f} C_{H^+}^3) \exp(n_{a3} \eta_c F/RT)} \quad (40)$$

$$\theta_{Pt\text{-}O_2}^0 = \frac{k_{1f}}{k_{1b}} C_{O_2} \theta_{Pt}^0 \quad (41)$$

$$\theta_{Pt\text{-}O_2H}^0 = \frac{k_{a3b}}{k_{a3f} C_{H^+}^3} \exp\left(\frac{n_{a3} \eta_c F}{RT}\right) \theta_{Pt}^0 \quad (42)$$

where θ_{Pt}^0, $\theta_{Pt\text{-}O_2}^0$, and $\theta_{Pt\text{-}O_2H}^0$ are the surface coverages of the corresponding species without contaminant.

Based on the proposed reaction mechanism, the changes in the surface coverages of Pt$_n$–P and Pt$_n$–P′ are given as

$$\begin{aligned}
\frac{d\theta_{Pt_n\text{-}P}}{dt} &= k_{p1f} C_P \theta_{Pt}^n - k_{p1b} \theta_{Pt_n\text{-}P} + k_{p2f} C_P \theta_{Pt\text{-}O_2}^n - k_{p2b} \theta_{Pt_n\text{-}P} C_{O_2}^n \\
&\quad + k_{ap3f} C_P \theta_{Pt\text{-}O_2H}^n C_{H^+}^3 \exp\left(-\frac{\alpha_{ap3} n_{ap3} \eta_c F}{RT}\right) \\
&\quad - k_{ap3b} \exp\left(\frac{(1-\alpha_{ap3}) n_{ap3} \eta_c F}{RT}\right) \theta_{Pt_n\text{-}P} \\
&\quad - k_{p4f} \exp\left(\frac{\alpha_{p4} q \eta_c F}{RT}\right) \theta_{Pt_n\text{-}P} \\
&\quad + k_{p4b} C_{H^+}^q \exp\left(\frac{-(1-\alpha_{p4}) q \eta_c F}{RT}\right) \theta_{Pt_n\text{-}P'} \\
&\quad - k_{p5f} \exp\left(\frac{\alpha_{p5} z \eta_c F}{RT}\right) \theta_{Pt_n\text{-}P} \\
&\quad + k_{p5b} C_{P'} C_{H^+}^z \exp\left(\frac{-(1-\alpha_{p5}) z \eta_c F}{RT}\right) \theta_{Pt}^n \\
&= -\left[k_{p1b} + k_{p2b} C_{O_2}^n + k_{ap3b} \exp\left(\frac{(1-\alpha_{ap3}) n_{ap3} \eta_c F}{RT}\right)\right. \\
&\quad \left. + k_{p4f} \exp\left(\frac{\alpha_{p4} q \eta_c F}{RT}\right) + k_{p5f} \exp\left(\frac{\alpha_{p5} z \eta_c F}{RT}\right)\right] \theta_{Pt_n\text{-}P} \\
&\quad + \left[k_{p1f} C_P A^n + k_{p2f} C_P B^n + k_{ap3f} C_P C_{H^+}^3 C^n \exp\right. \\
&\quad \times \left(-\frac{\alpha_{ap3} n_{ap3} \eta_c F}{RT}\right) + k_{p5b} C_{P'} C_{H^+}^z A^n \exp \\
&\quad \left. \times \left(\frac{-(1-\alpha_{p5}) z \eta_c F}{RT}\right)\right] (1 - \theta_{Pt_n\text{-}P} - \theta_{Pt_n\text{-}P'})^n \\
&\quad + k_{p4b} C_{H^+}^q \exp\left(\frac{-(1-\alpha_{p4}) q \eta_c F}{RT}\right) \theta_{Pt_n\text{-}P'} \quad (43)
\end{aligned}$$

and

$$\begin{aligned}
\frac{d\theta_{Pt_n\text{-}P'}}{dt} &= k_{p4f} \exp\left(\frac{\alpha_{p4} q \eta_c F}{RT}\right) \theta_{Pt_n\text{-}P} \\
&\quad - k_{p4b} C_{H^+}^q \exp\left(\frac{-(1-\alpha_{p4}) q \eta_c F}{RT}\right) \theta_{Pt_n\text{-}P'} \quad (44)
\end{aligned}$$

with the following initial conditions

$$\theta_{Pt_n\text{-}P}(t=0) = 0 \quad (45)$$

and

$$\theta_{Pt_n\text{-}P'}(t=0) = 0 \quad (46)$$

where t denotes time and C_P and $C_{P'}$ are the concentration of species P and P′, respectively. The cathode current density controlled by forward and backward rates of reaction (a-ii) [60] is calculated by

$$I_c = n_{O_2} F \gamma_c \left[k_{2f} \theta_{Pt\text{-}O_2} C_{H^+} \exp\left(-\frac{\alpha_2 n_2 \eta_c F}{RT}\right) - k_{2b} \theta_{Pt\text{-}O_2H} \exp\left(\frac{(1-\alpha_2) n_2 \eta_c F}{RT}\right)\right] \quad (47)$$

where n_{O_2} is the electron transfer number of the ORR and γ_c is the ratio of the active surface to the geometric surface of the CCL.

When there is no contamination, no current, and overpotential ($I_c = \eta_c = 0$), k_{2b} can be expressed from Eq. (47) as

$$k_{2b} = k_{2f}\frac{\theta^0_{Pt-O_2}}{\theta^0_{Pt-O_2H}}C_{H^+} \quad (48)$$

Substituting Eqs. (36)–(42) and (48) into Eq. (47) results in

$$I_c = n_{O_2}F\gamma_c k_{2f}\frac{k_{1f}}{k_{1b}}C_{O_2}AC_{H^+}\exp\left(-\frac{\alpha_2 n_2\eta_c F}{RT}\right) \times\left[1-\exp\left(\frac{n_2\eta_c F}{RT}\right)\right](1-\theta_{Pt_n-P}-\theta_{Pt_n-P'}) \quad (49)$$

The fuel cell voltage is estimated by

$$V_{cell} = V^0 - \eta_a - \eta_c - R_0 I_c \quad (50)$$

where V^0 is the open circuit voltage (OCV) of the fuel cell, η_a is the anode overpotential, and R_0 is the fuel cell internal resistance. The OCV is given by [61]

$$V^0 = 4.1868\left[\frac{70650 + 8T\log(T) - 92.84T}{2F}\right] \quad (51)$$

Anode over-potential is generally small compared to cathode overpotential and can be neglected:

$$\eta_a \approx 0 \quad (52)$$

Therefore, Eq. (50) can be rewritten as

$$V_{cell} = V^0 - \eta_c - R_0 I_c \quad (53)$$

2.3. Toluene contamination model

Several studies of toluene adsorption on Pt have been reported [62–67]. These demonstrate (1) that in the gas phase, toluene and benzene adsorb first as a π-complex (benzene ring parallel to the surface) with a weaker electron transfer to Pt as compared with ethane and propane [64]; (2) that an excess of the toluene can transform the π-complex into a σ-complex; and (3) that the substituent groups play an important role in the ordering of the overlayers but have less effect on the adsorption strength [62]. While adsorbed aromatic compounds are in an electrochemical environment, their molecular orientation and packing density depend on factors such as chemical composition, concentration, temperature, electrode potential, and the interaction between electrode and anions. The literature [68] suggests that all the aromatic compounds interact via their aromatic ring parallel to the Pt surface, the benzene and toluene mainly adsorbing without dissociation. One study [63] also indicated that the adsorbed toluene can be electrochemically oxidized partially to higher oxidation state intermediates and partially to CO_2.

To study the adsorption behaviour of toluene on Pt in conditions similar to those of fuel cell operation, a toluene adsorption isotherm study of polycrystalline platinum electrode was conducted [69]. It was found that the Langmuir type of adsorption fits well the adsorption isotherms in the studied temperature ranges (25–80 °C). The estimated free energy of adsorption revealed toluene's strong affinity towards the Pt surface; it was found that toluene adsorbed mainly as a σ-complex (vertical orientation) at low concentration and temperature, while the π-complex predominated at high concentration and particularly high temperatures.

Based on the experimental evidence, we propose that toluene adsorption (reaction (a-iv)) is the dominant mechanism for air-side toluene contamination in a fuel cell. At high electrode potential, toluene electrochemical oxidation takes place, which yields intermediates and carbon dioxides in higher oxidized states (as expressed in reactions (a-vii) and (a-viii)).

Toluene adsorption configuration is a complicated issue, strongly dependent on toluene concentration, temperature, and electrode potential. Vertical (σ) and flat (π) configurations are possible. Initially, we will consider only toluene adsorption as the dominant contamination mechanism. We start with the simplest single-site adsorption model.

In our model, oxygen pressure in the cathode catalyst layer, which is different from the pressure in the channel due to the pressure drop across the gas diffusion layer, is estimated by Fick's law as

$$p_{O_2} = 0.21(p_{CGC} - p^{sat}_{vapor}) - RT\frac{L_{CGDL}I_c}{4FD^{eff}_{O_2,air}} \quad (54)$$

where p_{O_2}, p_{CGC} and p^{sat}_{vapor} are the oxygen partial pressure, gas pressure in the gas channel, and saturated water vapor pressure, respectively, L_{CGDL} is the thickness of the cathode gas diffusion layer, and $D^{eff}_{O_2,air}$ is the effective oxygen diffusivity in air.

$$p^{sat}_{vapor} = \exp\left(11.6832 - \frac{3816.44}{T - 46.13}\right) \quad (55)$$

The effective oxygen diffusivity is estimated by the Bruggeman relation,

$$D^{eff}_{O_2,air} = (\varepsilon_{CGDL})^{1.5}D_{O_2,air} \quad (56)$$

where ε_{CGDL} is the porosity of the cathode gas diffusion layer and $D_{O_2,air}$ is the bulk oxygen diffusivity in air.

The oxygen concentration in the cathode catalyst layer is calculated by the gas law

$$C_{O_2} = \frac{p_{O_2}}{RT} \quad (57)$$

3. Experimental results

The testing platform design for fuel cell toluene contamination has been described in another paper [70]. All tests were conducted on a Fideris 100 W fuel cell test station with a single-cell hardware purchased from Teledyne (50 cm^2 CH-50). The flow field plates were designed and fabricated in-house using single serpentine flow channels of 1.2 mm width, 1.0 mm channel depth, and 1.0 mm landing. The membrane electrode assembly (MEA) has an active area of 50 cm^2. The gas diffusion layer (GDL), purchased from SGL Carbon Group, was a PTFE (20 wt%) and carbon black impregnated carbon paper. The catalyst coated membrane (CCM) (manufactured by Ion Power) was made of Nafion® 211 membrane with 0.4 mg cm^{-2} Pt loading on both anode and cathode sides. A fresh MEA was employed for each contamination test.

In all fuel cell tests both with and without toluene present, the voltage-current polarization curves (steady-state polarization curves) were collected using a load bank controlled in a constant-current pattern. The relative humidity (RH) of the fuel cell was controlled at 80% for both anode and cathode sides, and the cell temperature and backpressure were controlled at 80 °C and 30 psig, respectively.

4. Results and discussion

4.1. ORR parameter study

In order to obtain ORR parameters, we simulated experimental baseline data, which is free of contaminants. The parameters employed for the simulation are listed in Table 1, and the simulation and experimental polarization curves are illustrated in Fig. 1.

Table 1
Parameter values used in polarization fitting.

F	96485 C mol^{-1}
R	8.315 J K^{-1} mol^{-1}
T	353 K
n_{O_2}	4
γ_c	5000 cm^2 cm^{-2}
η_a	0 V
n	1
n_2	1
n_{a3}	1
α_{ap3}	0.5
n_{ap3}	1
α_{p4}	0.5
q	1
α_{p5}	0.5
z	1
L_{CGDL}	3.53×10^{-2} cm
p_{CGC}	30 psig
$D_{O_2,air}$	1.366×10^{-1} cm^2 s^{-1}
ε_{CGDL}	0.8
C_{H^+}	1.7273×10^{-3} mol cm^{-3}

Table 2
Estimated parameter values based on the baseline polarization curve.

$\frac{k_{1f}}{k_{1b}}$	5.8×10^4 cm^3 mol^{-1}
$\frac{k_{a3f}}{k_{a3b}}$	5.52×10^4 (cm^3)^3 (mol^{-1})^3
k_{2f}	1.64×10^{-11} s^{-1} cm^3 mol^{-1}
α_2	0.815

Table 2 lists the estimations of these parameters from the simulation. Our estimated rate constant for the rate-determining step (reaction (a-ii)) is 1.64×10^{-11}. This number is quite similar to the rate constant of 2.54×10^{-11}, which is derived from a reported experimental exchange current density obtained at fuel cell operating conditions in a high current density region, with a temperature of 80 °C [71]. The estimated symmetric parameter for the same reaction (α_2) is 0.815.

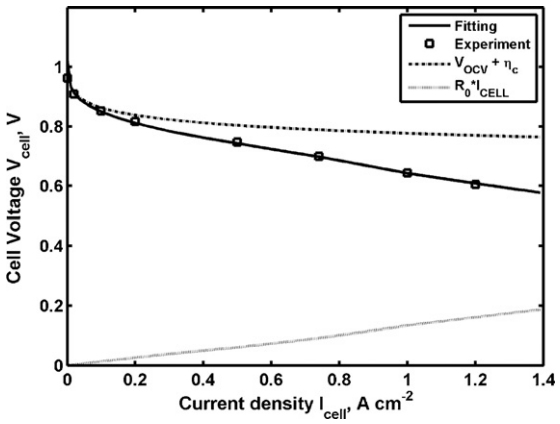

Fig. 1. Comparison of calculated and experimental polarization curve in the absence of contaminant.

As discussed in another paper [38], feed stream contaminant concentration at the catalyst layer is a function of both inlet contaminant concentration and current density. Furthermore, the contaminant adsorption (desorption) rate constant is also related to electrode potential. We can treat the product of the contaminant adsorption (desorption) rate constant and the contaminant concentration at the CCL as a function of current density and contaminant inlet concentration ($kC_P \sim f(C_P^0, I)$), where C_P^0 is the contaminant concentration in the cathode channel. With parametric study of experimental data at current densities of 0.2, 0.5, 0.75 and 1 A cm^{-2} and contaminant concentrations of 1, 5, and 10 ppm (Fig. 2), we have

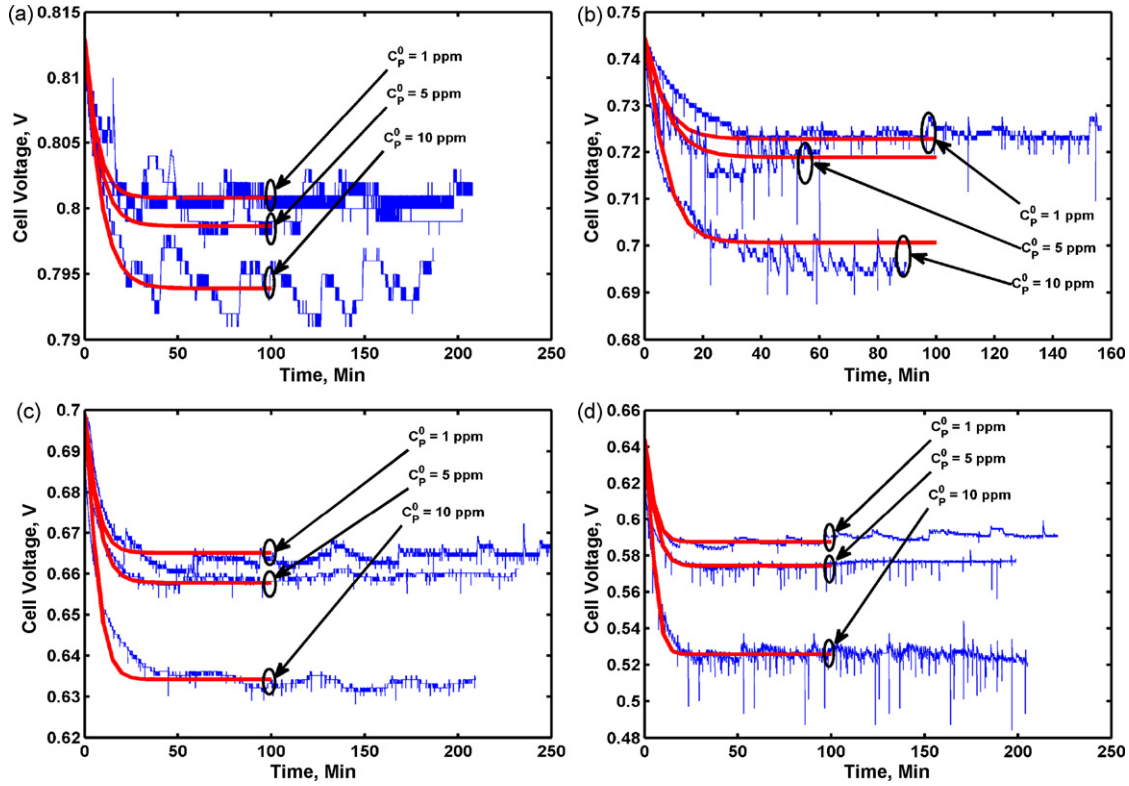

Fig. 2. Experimental performance data and modeling results at different toluene concentrations and different current densities: (a) I_{cell} = 0.2 A cm^{-2}; (b) I_{cell} = 0.5 A cm^{-2}; (c) at I_{cell} = 0.75 A cm^{-2} and (d) I_{cell} = 1.0 A cm^{-2}.

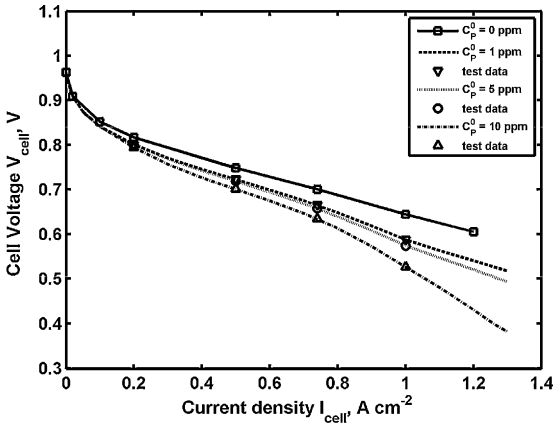

Fig. 3. Comparison of simulated and experimental steady-state performance under different toluene contaminations.

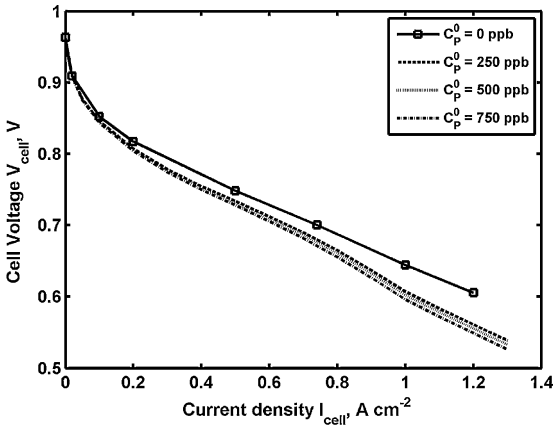

Fig. 5. Effects of toluene contaminations on steady-state fuel cell performance.

obtained a relationship between contaminant adsorption (desorption) rate constants, toluene concentration at the CCL, and current density that enables us to predict cell performance and surface coverage. Fig. 3 presents a comparison of steady-state cell performance under different toluene concentration levels.

4.2. Model simulation

With the developed toluene contamination model, we simulated transient and steady-state cell performance (Figs. 4 and 5) at different current densities and with toluene concentrations at ppb levels, which closely resemble normal indoor and outdoor toluene levels. As presented in Fig. 4, at a current density of 0.2 A cm^{-2} the voltage drop due to the presence of 750 ppb toluene can be 9 mV. If the current density is increased to 0.5, 0.75 and 1.0 A cm^{-2}, the same amount of toluene can cause corresponding cell performance drops up to 16, 27, and 48 mV, respectively. As shown in Fig. 4(d), at a current density of 1.0 A cm^{-2}, the cell voltage drops due to toluene concentrations of 250, 500 and 750 ppb are 37, 42 and 48 mV, respectively. Fig. 5 shows the effects of toluene contamination on steady-state cell performance at different concentration levels. Thus, the extent to which toluene contamination affects cell performance depends on toluene concentration and current density. Based on this model, we can estimate the maximum allowable toluene concentration in order to limit the voltage drop to a certain range. For instance, to limit the contamination potential drop to less than 10 mV, with a current density of 1.0 A cm^{-2}, toluene concentration should be less than 100 ppb. One can also estimate the degree of cell performance degradation at a certain contaminant level and current density.

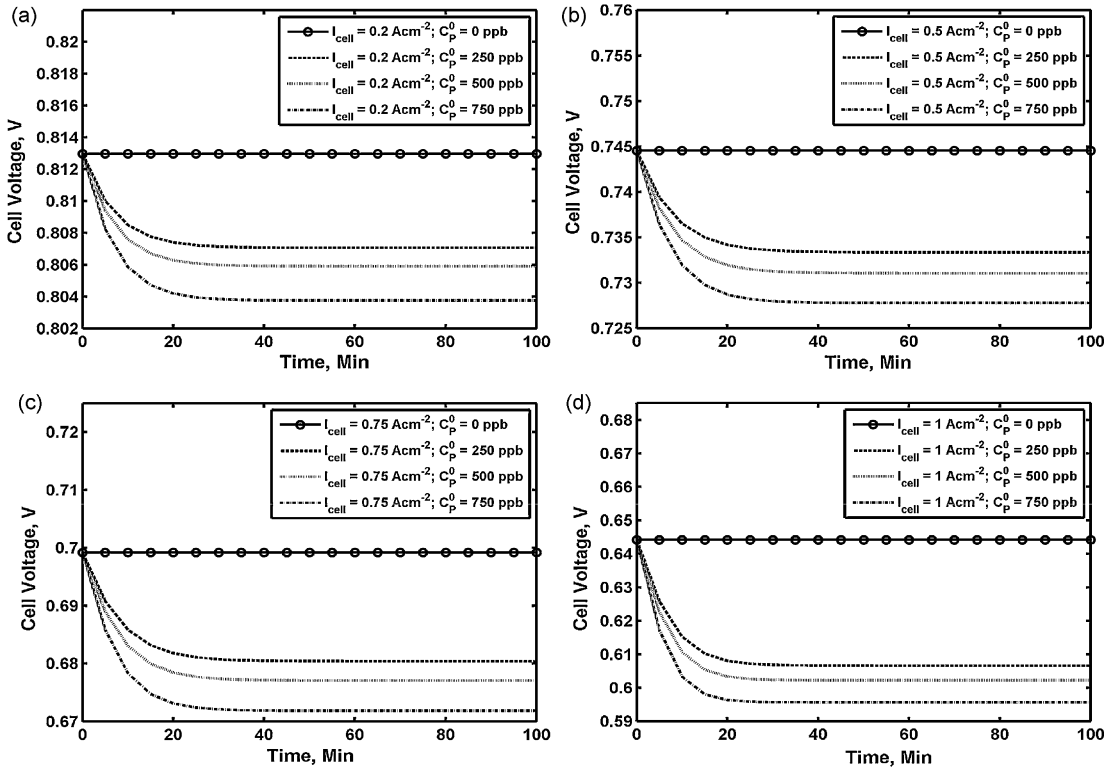

Fig. 4. Simulated fuel cell transient performance at different current densities and different toluene concentrations.

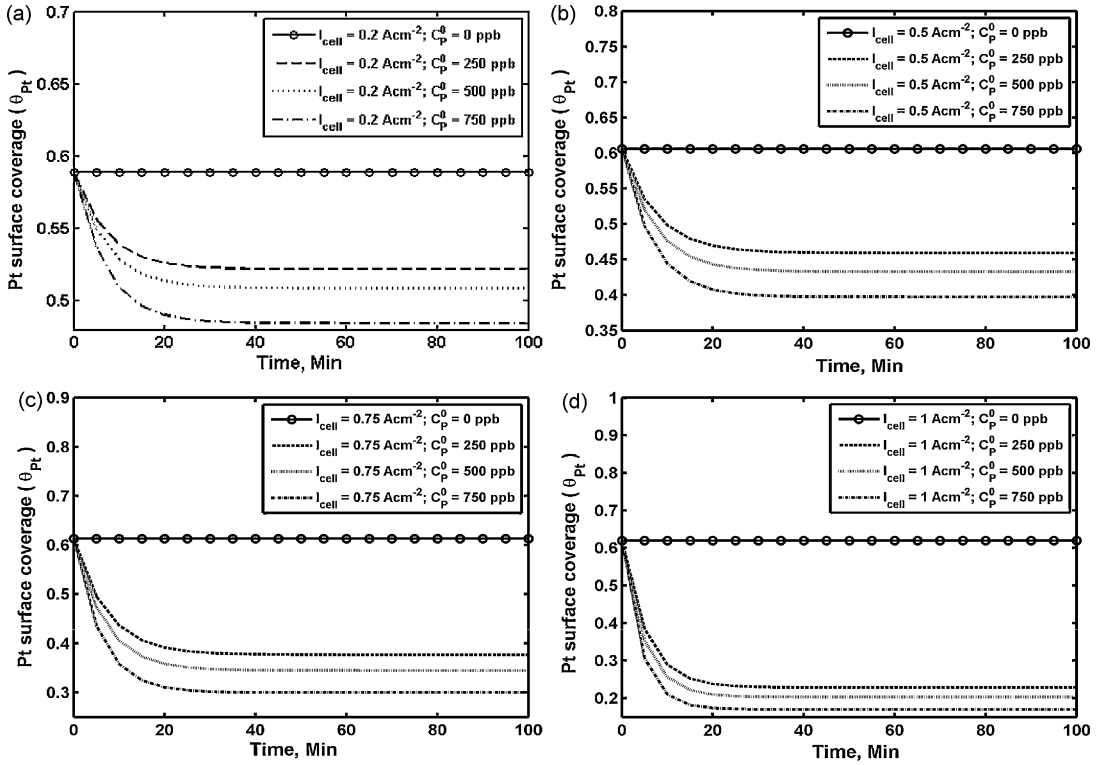

Fig. 6. Pt surface coverages at different current densities and different toluene concentrations.

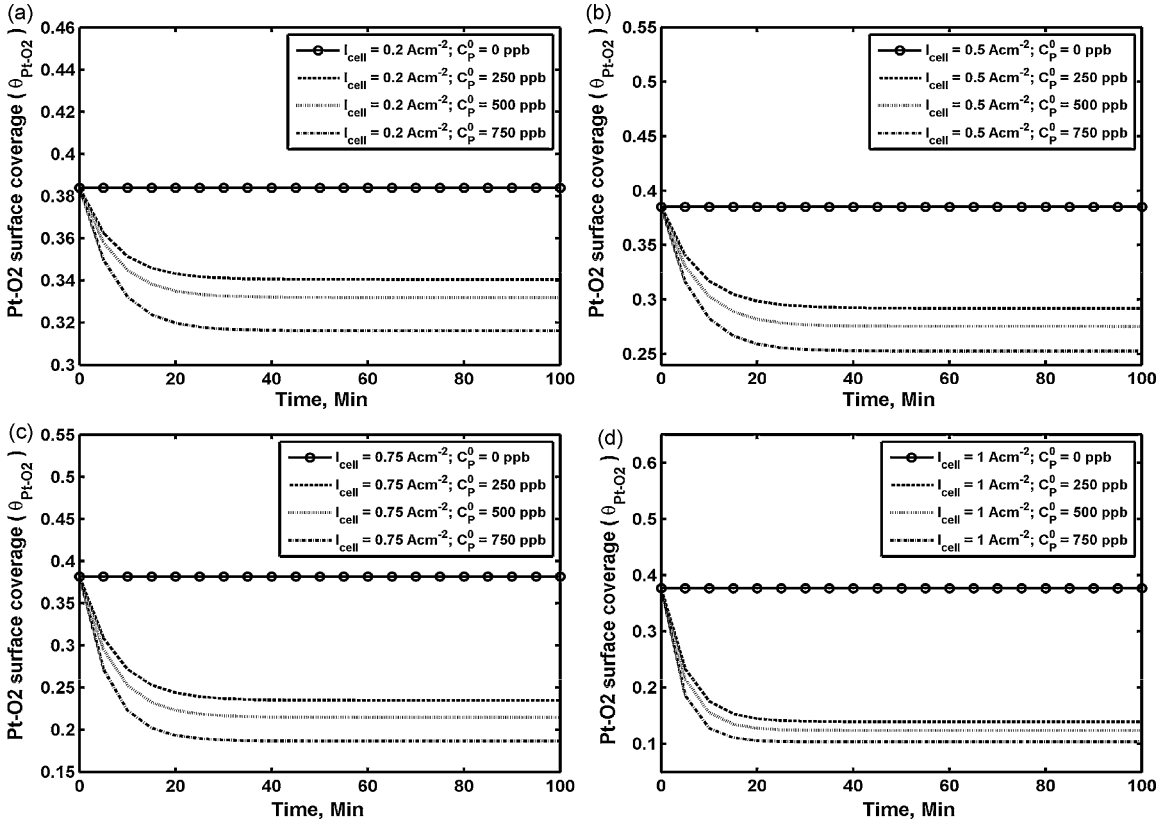

Fig. 7. Oxygen surface coverages at different current densities and different toluene concentrations.

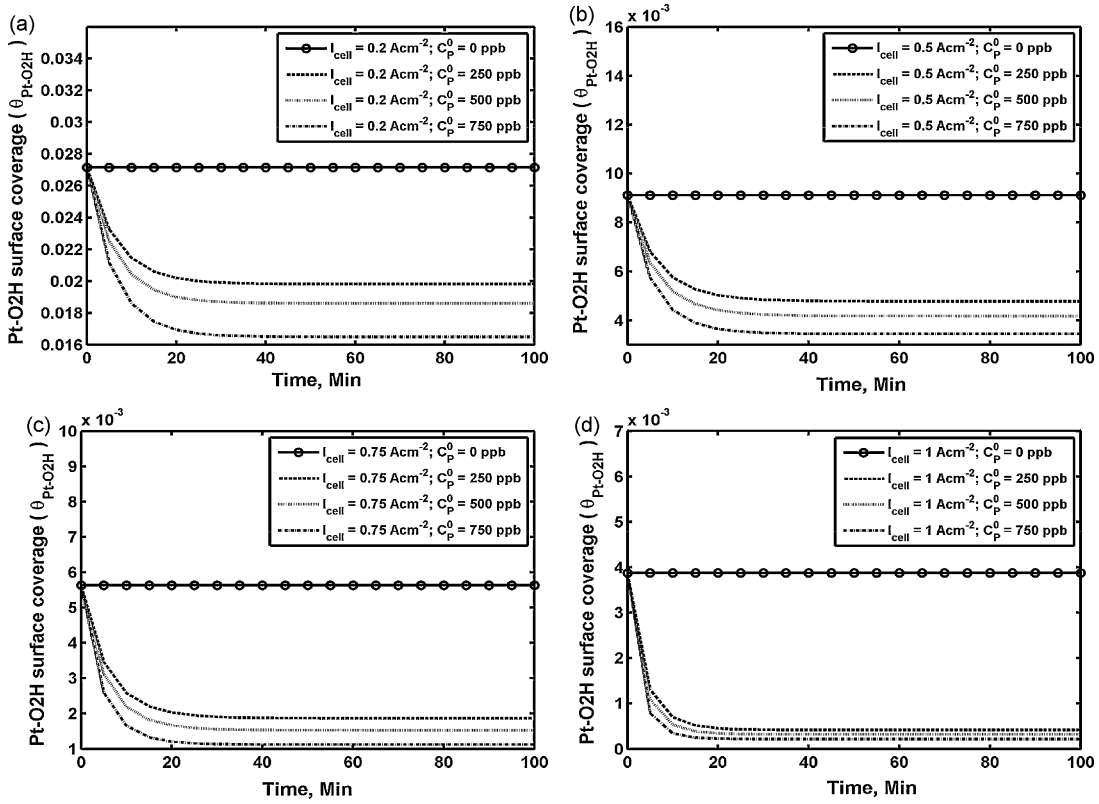

Fig. 8. Oxygen-containing intermediates surface coverages at different current densities and different toluene concentrations.

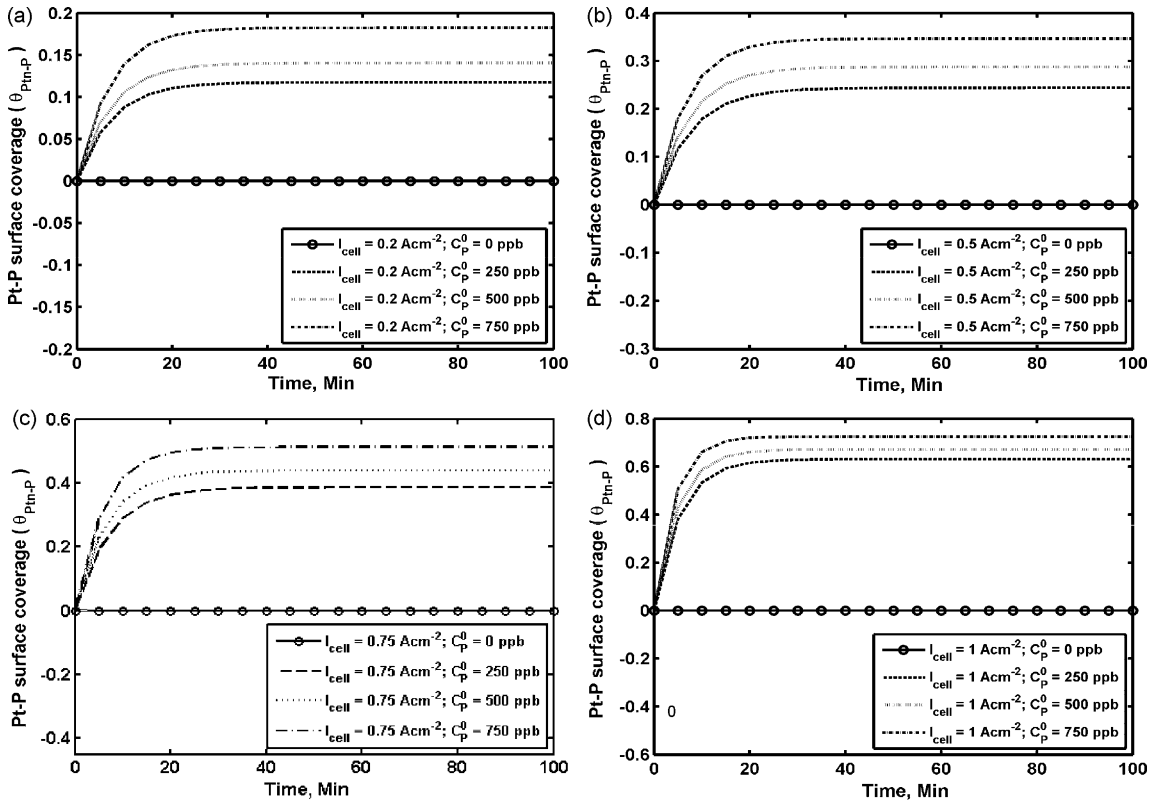

Fig. 9. Toluene surface coverages at different current densities and different toluene concentrations.

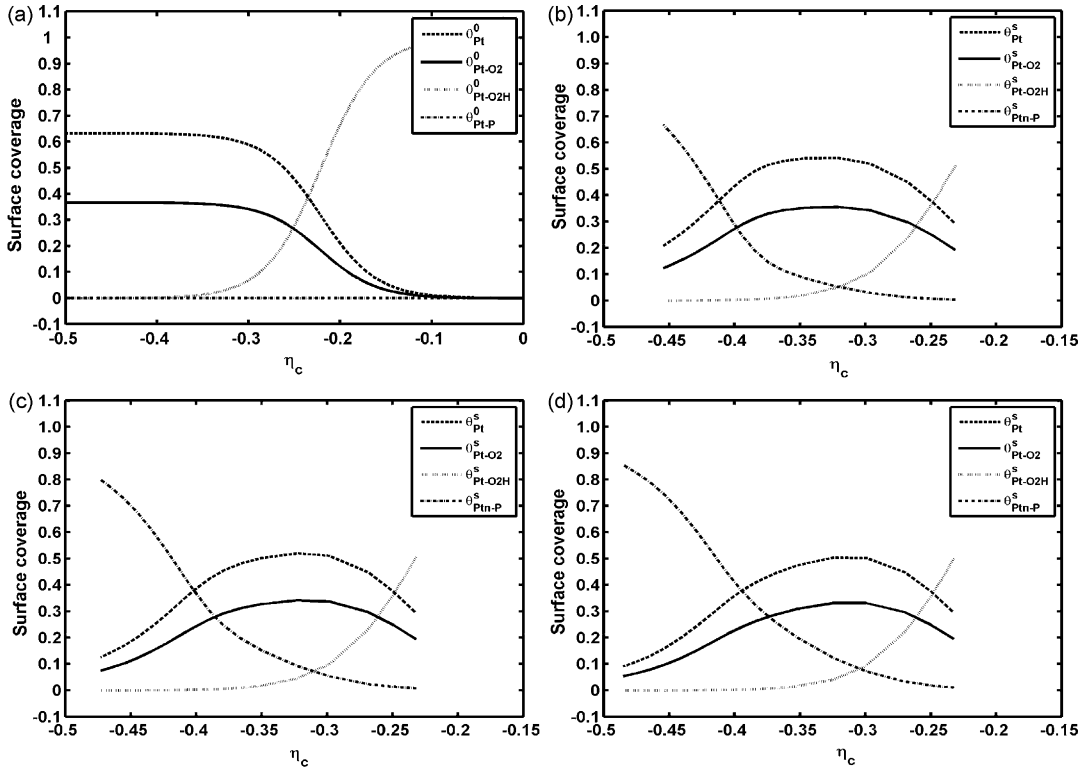

Fig. 10. Surface coverage variation with overpotential at different toluene concentrations: (a) $C^0_P = 0$ ppb; (b) $C^0_P = 250$ ppb; (c) $C^0_P = 500$ ppb; (d) $C^0_P = 750$ ppb.

With our model, we investigated the effect of toluene contamination on surface coverage at different current densities. The simulation results are illustrated in Figs. 6–9. Fig. 6 demonstrates the effect of contaminant level and current density on Pt surface coverage, θ_{Pt}. Two observations can be drawn from this figure: (1) the free Pt site coverage decreases as contamination level increases, indicating that toluene contamination blocks the free Pt sites; (2) with the same toluene concentration, increasing current density will result in a low number of free Pt sites. For example, at a current density of 0.2 A cm^{-2}, the free Pt site coverage is reduced from 59% to 48% as the toluene concentration increases from 0 to 750 ppb, while at a current density of 0.5 A cm^{-2}, the free Pt site coverage changes from about 60% to about 40%. The same observation can be made of Fig. 7, which simulates the surface coverage θ_{Pt-O_2}. Fig. 8 reveals the effects of current density and contaminant level on oxygen-containing intermediates coverage, θ_{Pt-O_2H}. At the current densities presented in this figure, the oxygen-containing intermediates coverage is small, as the subsequent reactions are much faster than its formation. Toluene contamination further reduces the coverage, and the extent of the effect is greater with a higher toluene concentration. With respect to contaminant surface coverage, Fig. 9 illustrates that increasing the contamination level and current density will in both cases increase the contaminant coverage, θ_{Pt-P}. Depending on the current density, with 750 ppb toluene the θ_{Pt-P} can be as high as 73%, suggesting a significant degradation in cell performance.

We also examined the surface coverage of all the species at different overpotentials and with different toluene concentrations (Fig. 10). When contaminant is absent, our simulation shows that in the overpotential range from 0 to 0.23 V the catalyst surface is covered mainly (coverage >50%) by oxygen-containing intermediates, θ_{Pt-O_2H}. From our model simulation, at an overpotential of around 0.29 the oxygen-containing intermediate coverage is about 10%. The same coverage was reported as well at a cell potential of 0.84 V [40]. Furthermore, at an overpotential greater than 0.26 V, the free Pt sites dominate (i.e., coverage >50%). Oxygen coverage (θ_{Pt-O_2}) is also generally less than half of the free Pt site coverage.

When toluene is present, we observe that at low overpotentials (less than 0.25 V), the toluene coverage (θ_{Pt-P}) is small regardless of toluene concentration. This is consistent with experimental observation [70] that toluene contamination has an insignificant effect on OCV. Significant toluene coverage (>10%) is mainly observed at large cathode overpotentials (>0.32 V). With higher toluene levels, significant toluene coverage will appear at relatively lower overpotentials. With 750 ppb toluene, 10% toluene coverage is noticed at a cathode overpotential >0.30 V. In addition, with the presence of contaminant we see a narrowing of the potential window in which free Pt sites dominate. With 0 ppb toluene, this free Pt site window is at an overpotential >0.26 V; with 250 ppb toluene, the window is >0.26 V and <0.38 V (0.12 V range); with 500 ppb, the window is >0.26 V and <0.37 V (0.11 V range); and with 750 ppb toluene, the window is >0.27 V and <0.36 V (0.09 V range). Thus, contamination significantly reduces the potential range in which free Pt sites dominate. As a result, the fuel cell's performance is adversely affected.

4.3. Model limitation

In this first general air-side contamination model, we have considered oxygen adsorption on a single Pt reaction active site to avoid mathematical challenges. While oxygen adsorption on Pt initially forms an end-on configuration, it then develops a bridged configuration, which may occupy two or more Pt sites. How the other site model fits the experimental data definitely requires more investigation. With respect to a toluene contamination model, toluene adsorption studies indicate that the adsorbate configuration is dependent on toluene concentration, temperature, and electrode potential. Further examination of the number of adsorption sites is

underway in our lab. It is known that the ORR rate depends on the Pt crystalline faces, as does the toluene adsorption rate. This rate difference and interplay may be one reason why overall, our simple adsorption models fit the experimental data. Furthermore, in reality toluene concentration in air is at the ppb level, so experimental validation at the ppb level is in progress at our lab.

5. Summary

We successfully developed a general air-side feed stream contamination model, which has been validated with experimental data on fuel cell toluene contamination at four different current densities (0.2, 0.5, 0.75, and 1 A cm^{-2}) and three toluene concentrations (1, 5, and 10 ppm). This model employs the associative oxygen reduction mechanism and considers possible contaminant reactions, such as surface adsorption, competitive adsorption, and electrochemical oxidation. The model has the capability to simulate and predict both transient and steady-state cell performance. Using it we examined toluene contamination effects on cell performance. Our model reveals that with 750 ppb toluene, a 48-mV performance drop at 1 A cm^{-2} can be expected. The contamination level and current density determine the extent of performance degradation. Our model simulation indicates that without contaminant, the oxygen-containing species dominate the catalyst surface at overpotentials <0.25 V. At overpotentials >0.26 V, free Pt sites dominate. In the presence of toluene contaminants, the surface coverage is not affected at low overpotentials (<0.25 V). Toluene contamination dominates at larger overpotentials (>0.3 V). With 750 ppb toluene, 20% toluene coverage is predicted at cathode overpotentials >35 V, while 50% coverage is predicted at overpotentials >0.40 V.

Acknowledgment

We would like to acknowledge support for this research from the National Research Council of Canada, Institute for Fuel Cell Innovation (NRC-IFCI).

References

[1] P.R. Hayter, P. Mitchell, R.A.J. Dams, C. Dudfield, N. Gladding, The effect of contaminants in the fuel and air streams on the performance of a solid polymer fuel cell, Contract Report (ETSUF/02/00126/REP) Wellman CJB Limited, Portsmouth, UK, 1997.
[2] D. Brumbaugh, J. Guthrie, Literature Survey of Fuel Cell Contaminants, US Fuel Cell Council (Ed), US Fuel Cell Council, 2004.
[3] X. Cheng, Z. Shi, N. Glass, L. Zhang, J. Zhang, D. Song, Z.S. Liu, H. Wang, J. Shen, J. Power Sources 165 (2007) 739.
[4] H.P. Dhar, L.G. Christner, A.K. Kush, J. Electrochem. Soc. 134 (1987) 3021.
[5] H.F. Oetjen, V.M. Schmidt, U. Stimming, F. Trila, J. Electrochem. Soc. 143 (1996) 3838.
[6] C. Sishtla, G. Koncar, R. Platon, S. Gamburzev, A.J. Appleby, O.A. Velev, J. Power Sources 71 (1998) 249.
[7] F.A. Uribe, T.A. Zawodzinski, Electrochemical Society Meeting Abstract, San Francisco, 2001.
[8] F.A. Uribe, S. Gottesfeld, T.A. Zawodzinski, J. Electrochem. Soc. 149 (2002) A293–A296.
[9] F.A. de Bruijn, D.C. Papageorgopoulos, E.F. Sitters, G.J.M. Janssen, J. Power Sources 110 (2002) 117.
[10] N. Rajalakshmi, T.T. Jayanth, K.S. Dhathathreyan, Fuel Cell 3 (4) (2003) 177–180.
[11] R. Halseid, J.S. Preben Vie, R. Tunold, J Power Sources 154 (2006) 343.
[12] M. Murthy, M. Esayian, A. Hobson, S. MacKenzie, W.-k. Lee, J.W. Van Zee, J. Electrochem. Soc. 148 (2001) A1141–A1147.
[13] M. Murthy, M. Esayian, W.-k. Lee, J.W. Van Zee, J. Electrochem. Soc. 150 (2003) A29–A34.
[14] R. Mohtadi, W.-k. Lee, S. Cowan, J.W. Van Zee, M. Murthy, Electrochem. Solid-State Lett. 6 (2003) A272–A274.
[15] R. Mohtadi, W.K. Lee, J.W. Van Zee, Appl. Catal. B: Environ. 56 (2005) 37.
[16] S. Knights, N. Jia, C. Chuy, J. Zhang, 2005 Fuel Cell Seminar: Fuel Cell Progress, Challenges and Markets Abstract, Palm Springs, 2005.
[17] W. Shi, B. Yi, M. Hou, F. Jing, H. Yu, P. Ming, J. Power Sources 164 (2007) 272.
[18] R.K. Ahluwalia, X. Wang, J. Power Sources 180 (2008) 122.
[19] R.J. Behm, Z. Jusys, J. Power Sources 154 (2006) 327.
[20] A.K. Meland, S. Kjelstrup, J. Electroanal. Chem. 610 (2007) 171.
[21] D. Yang, J. Ma, L. Xu, M. Wu, H. Wang, Electrochim. Acta 51 (2006) 4039.
[22] R. Mohtadi, W. Lee, J.W. Van Zee, J. Power Sources 138 (2004) 216.
[23] F. Jing, M. Hou, W. Shi, J. Fu, H. Yu, P. Ming, B. Yi, J. Power Sources 166 (2007) 172.
[24] Y. Garsany, O.A. Baturina, K.E. Swider-Lyons, J. Electrochem. Soc. 154 (2007) B670–B675.
[25] J.M. Moore, P.L. Adcock, J.B. Lakeman, G.O. Mepsted, J. Power Sources 85 (2000) 254.
[26] T. Springer, T. Zawodzinski, S. Gottesfeld, in: J. McBreen, S. Mukherjee, S. Srinivasan (Eds.), Proceedings of the Symposium on Electrode Material and Processes for Energy Conversion and Storage IV, Pennington, NJ, Electrochemical Society, Inc. 1997.
[27] T.E. Springer, T. Rockward, T.A. Zawodzinski, S. Gottesfeld, J. Electrochem. Soc. 148 (2001) A11–A23.
[28] X. Wang, I.M. Hsing, Y.J. Leng, P.L. Yue, Electrochim. Acta 46 (2001) 4397.
[29] P. Rama, R. Chen, R. Thring, Proceedings of the Institution of Mechanical Engineers, Part A, J. Power Energy, 219 (2005) 255.
[30] K.K. Bhatia, C.-Y. Wang, Electrochim. Acta 49 (2004) 2333.
[31] J.J. Baschuk, A.M. Rowe, X. Li, J. Energy Res. Technol. 125 (2003) 94.
[32] J.J. Baschuk, Xianguo Li, Int. J. Global Energy Issues 20 (2003) 245.
[33] S.H. Chan, S.K. Goh, S.P. Jiang, Electrochim. Acta 48 (2003) 1905.
[34] J. Zhang, H. Wang, D.P. Wilkinson, D. Song, J. Shen, Z.-S. Liu, J. Power Sources 147 (2005) 58.
[35] A.A. Shah, P.C. Sui, G.S. Kim, S. Ye, J. Power Sources 166 (2007) 1.
[36] D.J.L. Brett, P. Aguiar, N.P. Brandon, A.R. Kucernak, Int. J. Hydrogen Energy 32 (2007) 863.
[37] C.G. Farrell, C.L. Gardner, M. Ternan, J. Power Sources 171 (2007) 282.
[38] Z. Shi, D. Song, J. Zhang, Z.S. Liu, S. Knights, R. Vohra, N. Jia, D. Harvey, J. Electrochem. Soc. 154 (2007) B609–B615.
[39] J. St-Pierre, N. Jia, R. Rahmani, J. Electrochem. Soc. 155 (2008) B315–B320.
[40] A. Damjanovic, M.A. Genshaw, Electrochim. Acta 15 (1970) 1281.
[41] K. Kinoshita, in: K. Kinoshita (Ed.), Electrochemical Oxygen Technology, John Wiley & Sons, Inc., New York, 1992, Ch. 2.
[42] R. Adzic, in: J. Lipkowski, P.N. Ross (Eds.), Electrocatalysis, Wiley-VCH, New York, 1998, Ch. 5.
[43] M. Gattrell, B. MacDougall, in: W. Vielstich, H.A. Gasteiger, A. Lamm (Eds.), Handbook of Fuel Cells—Foundamentals, Technology and Applications; vol. 2: Electrocatalysis, John Wiley & Sons, 2003, Ch. 30.
[44] P.N. Ross Jr., in: W. Vielstich, H.A. Gasteiger, A. Lamm (Eds.), Handbook of Fuel Cells—Foundamentals, Technology and Applications, vol. 2: Electrocatalysis, John Wiley & Sons, 2003, Ch. 31.
[45] A. Damjanovic, V. Brusic, Electrochim. Acta 12 (1967) 615.
[46] D.B. Sepa, M.V. Vojnovic, Lj. M. Vracar, A. Damjanovic, Electrochim. Acta 32 (1987) 129.
[47] E. Yeager, M. Razaq, D. Gervasio, A. Razaq, D. Tryk, in: D. Scherson, D. Tryk, M. Daroux, X. Xing (Eds.), Structure Effects in Electrocatalysis and Oxygen Electrochemistry, Proc. Vo. 92-11, The Electrochem. Soc. Inc., Pennington, NJ, 1992, p. 440.
[48] O. Antoine, Y. Bultel, R. Durand, J. Electroanal. Chem. 499 (2001) 85.
[49] H. Kuhn, A. Wokaun, G.G. Scherer, Electrochim. Acta 52 (2007) 2322.
[50] C.Y. Du, T.S. Zhao, C. Xu, J. Power Sources 167 (2007) 265.
[51] V.P. Zhdanov, B. Kasemo, Electrochem. Commun. 8 (2006) 1132.
[52] Z. Shi, J. Zhang, Z.S. Liu, H. Wang, D.P. Wilkinson, Electrochim. Acta 51 (2006) 1905.
[53] Z. Shi, in: J. Zhang (Ed.), PEM Fuel Cell Electrocatalysts and Catalyst Layer, Springer, 2008, Ch. 5.
[54] A.B. Anderson, T.V. Albu, J. Electrochem. Soc. 147 (2000) 4229.
[55] R.A. Sidik, A.B. Anderson, J. Electroanal. Chem. 528 (2002) 69.
[56] J.K. Norskov, J. Rossmeisl, A. Logadottir, L. Lindqvist, J.R. Kitchin, T. Bligaard, H. Jonsson, J. Phys. Chem. B 108 (2004) 17886.
[57] G.S. Karlberg, J. Rossmeisl, J.K. Norskov, Phys. Chem. Chem. Phys. 9 (2007) 5158.
[58] T. Jacob, Fuel Cell 6 (2006) 159.
[59] S. Walch, A. Dhanda, M. Aryanpour, H. Pitsch, J. Phys. Chem. C 112 (2008)8464.
[60] J. Newman, K.E. Thomas-Alyea, Electrochemical Systems, John Wiley & Sons, 2004, p. 210.
[61] A.E. Weber, R.M. Darling, J. Newman, J. Electrochem. Soc. 151 (2004) A1715.
[62] J.L. Gland, G.A. Somorjai, Surf. Sci. 41 (1974) 387.
[63] J. Zhu, T. Hartung, D. Tegtmeyer, H. Baltruschat, J. Heitbaum, J. Electroanal. Chem. 244 (1988) 273.
[64] Z. Hlavathy, P. Tetenyi, Appl. Surf. Sci. 252 (2005) 412.
[65] M.C. Tsai, E.L. Muetterties, J. Am. Chem. Soc. 104 (1982) 2534.
[66] S. Chiang, Chem. Rev. 97 (1997) 1083.
[67] A.T. Hubbard, Chem. Rev. 88 (1988) 633.
[68] J.L. RodrØguez, E. Pastor, Electrochim. Acta 45 (2000) 4279.
[69] K. Fatih, H. Wang, Z. Shi, D. Song, H. Li, J. Zhang, W. Shaohong, J. Zhang, Electrochim. Acta, submitted for publication.
[70] H. Li, J. Zhang, K. Fatih, Y. Tang, Z. Wang, Z. Shi, W. Shaohong, D. Song, J. Zhang, N. Jia, S. Wessel, R. Abouatallah, N. Joos, J. Power Sources 185 (2008) 272.
[71] C. Song, Y. Tang, J.L. Zhang, J. Zhang, H. Wang, J. Shen, S. McDermid, J. Li, P. Kozak, Electrochim. Acta 52 (2007) 2552.